Scattering and Absorption by Thin Metal Wires in Rectangular Waveguide—FDTD Simulation and Physical Experiments

Marianne Bingle, David Bruce Davidson, and Johannes Hendrik Cloete

***Abstract*—The high-frequency internal impedance model of a round ohmic conductor is incorporated into the subcell thin-wire formulation of the finite-difference time-domain method to model the microwave properties of metal wires. For magnetic metals, such as steel, an effective conductivity is introduced to account for the increase in ohmic loss due to the high-frequency permeability. Physical experiments with half-wave resonant copper- and steel-wire inclusions, supported by a dielectric slab in a standard S-band rectangular waveguide, support the formulation.**

***Index Terms*—FDTD, finite difference time domain, microwave absorber, ohmic conductors, thin wire.**

I. Introduction

WE HAVE developed a finite-difference time-domain (FDTD) code for the broad-band numerical simulation of scattering by conducting wires, supported by a dielectric host in a rectangular waveguide. The purpose of the code was to provide us with a numerical tool to study the absorption mechanisms at play in synthetic composites which employ thin metal wires in a lossy dielectric host [1]–[3]. We specifically studied arrangements of hooked metal-wire inclusions in unit cells, as shown, for example, in Fig. 1(a) and (b), for reasons not essential to this paper, but briefly alluded to in Section IV.

Wires are assumed to be "perfect" electrical conductors in the FDTD subcell thin-wire formulation of Umashankar *et al.* [4]. However, the finite conductivity of physical metals can significantly influence the way in which wires scatter and absorb electromagnetic waves in the microwave regime. In an otherwise essentially transparent environment, the ohmic loss in a wire is not negligible about resonance and should be accounted for in a good numerical model [2], [3].

We describe how to account for the relevant microwave properties of metal wires, made of copper and steel, for example, through the incorporation of a high-frequency internal impedance model of a round conductor into the standard subcell thin-wire formulation. In the case of steel, which is magnetic, an effective conductivity is introduced to account for the permeability of the metal at microwave frequencies. The model allows for the wires to be supported by a dielectric, such as a slab of low-loss polystyrene foam or nonmagnetic absorbing material.

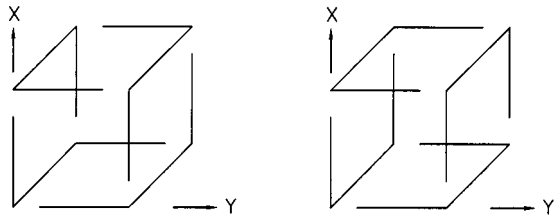

(a) (b)

Fig. 1. Unit cells of metal-wire hooks of resonant length in the microwave regime embedded in a dielectric host. (a) Unit cell of cranks (chiral hooks). (b) Unit cell of staples (nonchiral hooks).

We briefly describe a mechanism to accurately compute the incident E- and H-field time pulses of the TE_{10} mode for the broad-band excitation of a rectangular waveguide in a total-field/scattered-field [5] FDTD algorithm.

The code was validated against physical experiments performed in a standard S-band (nominally 2.6–3.95 GHz) rectangular waveguide. A selection of these results is presented and discussed.

II. FDTD Formulation

A. Physical Basis of the Formulation to Simulate Propagation in a Dielectric Medium

A class of nonmagnetic microwave absorbing materials, which was developed at the University of Stellenbosch, Stellenbosch, South Africa [6] can be characterized to a good approximation by a frequency-dependent complex, relative permittivity $\epsilon_r(\omega)$, and a frequency-independent (up to infrared frequencies) ohmic conductivity σ.

The material parameters of the absorbers are determined in the frequency domain from the measured scattering parameters of a homogeneous slab, either through a direct inversion technique or a model-based parameter-estimation technique [7]–[11].

A slab of microwave absorber was fitted tightly into an S-band rectangular waveguide for measurement of the scattering parameters. With the absorber's use restricted to the S-band, it can be characterized by a constant real permittivity $\epsilon_r \approx 1.67$ and a constant conductivity $\sigma \approx 0.04$ S/m. Uncertainties in the sample thickness, surface roughness of the sample, and a possible offset in the position of the sample add an error margin of approximately 10% on the estimated

Manuscript received February 4, 2000; revised February 15, 2001.

M. Bingle was with Department of Electrical and Electronic Engineering, University of Stellenbosch, Stellenbosch 7600, South Africa. She is now with Electromagnetic Software and Systems, Stellenbosch 7599, South Africa.

D. B. Davidson and J. H. Cloete are with the Department of Electrical and Electronic Engineering, University of Stellenbosch, Stellenbosch 7600, South Africa (e-mail: jhcloete@sun.ac.za).

Publisher Item Identifier S 0018-9480(02)05212-2.

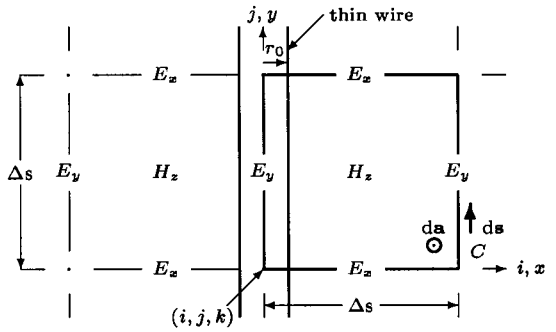

Fig. 2. Integration contour for discretization of Faraday's law in a Yee cell that contains a thin wire.

material parameters. The properties of a low-density low-loss polystyrene foam were estimated, also from S-band waveguide measurements, to be $\epsilon_r \approx 1.02$ and $\tan\delta < 0.001$ and could, therefore, realistically be modeled as air in the numerical simulations.

Maxwell's partial differential equations, combined with the local in time and space constitutive relations $\mathbf{D} = \epsilon_0\epsilon_r\mathbf{E}$ and $\mathbf{J} = \sigma\mathbf{E}$ are solved with the FDTD method [5]. Space and time are discretized after Yee, and Maxwell's partial differential equations approximated by central difference equations. The time evolution of the fields is computed at time steps Δt, which comply with the Courant stability criterion, and with a uniform spatial discretization Δs. The total-field/scattered-field formulation described in [5] is used.

B. Subcell Thin-Wire Formulation for Physical Conductors

A subcell thin-wire formulation was implemented in the code to model metal-wire inclusions in the FDTD geometry. Following Umashankar *et al.* [4], [12], the contour integral in Faraday's law is discretized in the cells containing a thin wire, and the integration is performed analytically to derive the update equations for the circumferential H-field components adjacent to the wire. The integration contour and surface are shown in Fig. 2. The wire is positioned at tangential E-field nodes in the Yee grid. (Update equations for a thin-wire bend of 90° were derived separately with the same field assumptions described below.)

In performing the integral, the radial E-field and the circumferential H-field components are assumed to have a $1/r$ spatial dependency near the wire. These are quasi-static approximations for the *scattered* radial E-field of an isolated infinitely long line-charge and the *scattered* circumferential H-field of an isolated infinitely long line current. They are, however, applied to the respective *total* field components, as suggested intuitively in [4] and [12]. We have found—from an analysis in which the update equations were derived with the $1/r$-approximation applied to the scattered field only—that the approximation applied instead to the total field yields negligible error for ratios of $(r_0/\Delta s)$ roughly between 0.1–0.3.

Other authors have introduced modifications to the local-field approximations to improve the accuracy [13], [14]. Note that the latter is specifically for radiation, not scattering, problems; the main improvement reported in [14] is an end-cap treatment.

In the formulation of Umashankar *et al.* [4], it is further assumed that the wire is a "perfect" conductor, and the axial E-field component in the wire is accordingly set to zero. However, in our research, we specifically wished to study the physical role of finite conductivity in the scattering and absorption by wire shapes, especially at resonance [1], [2].

Our approach is outlined here, using the following notation: the electromagnetic field and the current in the wire are interchangeably expressed with the same symbol in the time domain, frequency domain, and s-domain—the domain is indicated by the parameter t or ω or s, e.g., $E_y(r_0, t)$ is a real time-domain function, while $E_y(r_0, \omega)$ and $E_y(r_0, s)$ are complex, frequency-, and s-domain functions, respectively.

Electromagnetic fields penetrate into good conductors. A frequency-domain approximation relates the tangential E-field at the wire surface to the total current in the wire through an internal impedance

$$E_{\tan}(r_0, \omega) = Z_i(r_0, \omega) I(r_0, \omega). \tag{1}$$

The expression for the internal impedance of a uniform round conductor consists of complex Bessel functions of fractional complex argument [15, pp. 180–186]. The argument is proportional to r_0/δ, where $\delta = (\pi f\, \mu\sigma_{\text{wire}})^{-1/2}$ is the "skin depth," μ is the permeability, and σ_{wire} is the conductivity of the wire. The high-frequency approximation of this expression—corresponding to a large argument—is

$$Z_i(r_0, \omega)_{\text{hf}} \approx \frac{1}{2\pi r_0}\sqrt{\frac{j\omega\,\mu_0}{\sigma_{\text{wire}}}} \tag{2}$$

assuming the metal is nonmagnetic at microwave frequencies.[1] The expression in (2) is similar to the expression for the surface impedance of a conducting infinite half-space, which is used by Beggs *et al.* [16], [17] as a surface impedance boundary condition in the FDTD method.

By mathematically manipulating (1) and (2), and through analytic continuation $(j\omega \to s)$

$$E_{\tan}(r_0, s) = Z_i'(r_0, s) s I(r_0, s) \tag{3}$$

$$Z_i'(r_0, s) = \frac{1}{2\pi r_0}\sqrt{\frac{\mu_0}{\sigma_{\text{wire}}}}\frac{1}{\sqrt{s}}. \tag{4}$$

If the conductivity of the wire is frequency independent, $Z_i'(r_0, s)$ facilitates the transformation to the time domain, as in [16] and [17], by the Laplace transform pair $\mathcal{L}^{-1}(1/\sqrt{s}) = 1/\sqrt{\pi t}\,(t > 0)$ [18, p. 299]. The inverse Laplace transform of (3) relates the tangential E-field at the wire surface, in the time domain, by convolution to the time derivative of the current in the wire

$$E_{\tan}(r_0, t) = \frac{1}{2\pi r_0}\sqrt{\frac{\mu_0}{\pi\sigma_{\text{wire}}}}\int_0^t \frac{1}{\sqrt{t-\tau}}\frac{\partial I(r_0, \tau)}{\partial \tau}d\tau. \tag{5}$$

The convolution integral is discretized in time and written as the sum of integrals over intervals of Δt. The time derivative of the current is assumed piecewise constant over the discrete integration intervals and approximated by a backward difference

[1] Reference [15, Fig. 4.5(b)] compares the real and imaginary parts of the internal impedance to that of the high-frequency approximation.

equation from the center of the interval. In the discretized notation used below, the superscript n is the time index and the spatial index (i, j, k) refers to the FDTD cell associated with the field or current values, and is omitted in the equations. In thin-wire subcells, $E^n_{\tan}(r_0)$ in the discretized (5) provides the estimate for $E^n_{\tan}(i, j, k)$ on the axis. The update equation for the axial E-field component in the wire is a convolution sum, requiring knowledge of all previous current values

$$E^n_{\tan} = \frac{1}{2\pi r_0}\sqrt{\frac{\mu_0}{\pi\sigma_{\text{wire}}\Delta t}}\sum_{m=0}^{n-1} Z_0(n-m-1) \cdot \left(I^{m+(1/2)} - I^{m-(1/2)}\right) \tag{6}$$

$$Z_0(m) \equiv \int_m^{m+1} \frac{d\alpha}{\sqrt{\alpha}} = 2\left(\sqrt{m+1} - \sqrt{m}\right). \tag{7}$$

By expanding the discrete impulse response in an exponential series

$$Z_0(m) \approx \sum_{p=1}^{N} a_p e^{\alpha_p m} \tag{8}$$

the convolution sum can be performed recursively [16], [17]. The coefficients and exponents for a ten-term exponential series adequately approximating $Z_0(m)$—determined with Prony's method—are tabulated in [19, p. 174]. The update equation for the axial E-field becomes

$$E^n_{\tan} = \frac{1}{2\pi r_0}\sqrt{\frac{\mu_0}{\pi\sigma_{\text{wire}}\Delta t}}\sum_{p=1}^{10} \Psi^n_p \tag{9}$$

and $\Psi^n_p(i, j, k)$ is determined recursively from the current supported by the wire

$$\Psi^n_p = a_p \sum_{m=0}^{n-1} e^{(n-m-1)\alpha_p}\left(I^{(m+1/2)} - I^{(m-1/2)}\right) = e^{\alpha_p}\Psi^{n-1}_p + a_p\left(I^{(n-1/2)} - I^{(n-3/2)}\right) \tag{10}$$

where $\Psi^n_p(i, j, k) = 0$ for $n = 0, 1$.

Equation (9) accounts for the conductivity of physical wires, and is included into the update equations for the circumferential H-field components adjacent to the wire in the subcell thin-wire formulation. Ampère's contour integral was discretized along a rectangular loop around the wire to compute the current from the four circumferential H-field components, positioned half a cell from the wire axis in the Yee grid. The displacement current through the loop is neglected. Note that there are ten recursive convolution variables $\Psi^n_p(i, j, k)$ associated with each coordinate direction. The formulation can, therefore, substantially increase the requirement on memory resources.

C. Rectangular Waveguide Model and Pulsed Excitation

The rectangular waveguide model is shown in Figs. 3 and 4. It uses the total-field/scattered-field formulation [5]. The waveguide walls are assumed perfect; the waveguide lattice is terminated at both ends in Bérenger's perfectly matched layer (PML) absorbing boundary condition [20], [21], which has been shown

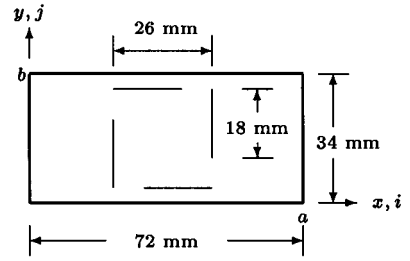

Fig. 3. Diagram of the front face of a unit cell in an S-band rectangular waveguide.

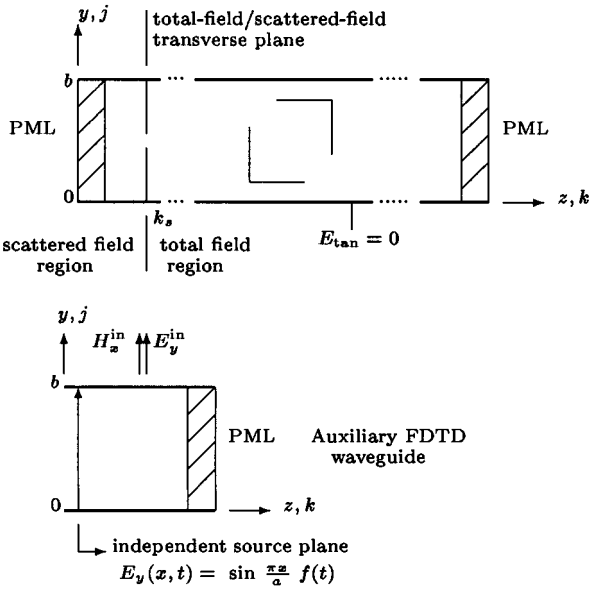

Fig. 4. Side-view diagram of the rectangular waveguide FDTD configuration (top), and the auxiliary waveguide model to compute the incident fields (bottom). The incident E- and H-field components of a broad-band waveguide mode are computed in the auxiliary waveguide, which is excited by an independent transverse plane source.

to efficiently absorb propagating waves in waveguide [22]. The PML is ineffective in absorbing evanescent waves or propagating waves close to cutoff [23], [24].

In order to achieve broad-band simulation, a pulsed incident wave is constructed for the total-field/scattered-field algorithm. Based on the concept of the one-dimensional source grid for unbounded space problems [5], the required incident E- and H-field pulses are computed (in parallel) in an auxiliary waveguide lattice [25] and introduced into the total-field/scattered-field algorithm. (Note that the E- and H-field pulses are related by convolution due to the frequency-dependent transverse-wave impedance of the waveguide mode [15, pp. 423–428]).

The auxiliary FDTD boundary value problem (see Fig. 4, bottom) resolves the incident E- and H-field time pulses numerically, with the appropriate time and spatial offsets of the FDTD discretization. It has the actual waveguide cross-sectional dimensions and is terminated a few cells ($3\Delta s$ in our simulations) from the source plane in a PML absorbing boundary. The TE_{10} mode is excited with an independent distributed source—also named an *electric wall* [26] or *hard source* [5, p. 109] in the literature—at a transverse plane in the auxiliary waveguide, $E_y(x,t) = \sin(\pi x/a)f(t)$. The

time dependence of the excitation is a modulated windowed sinusoidal carrier function with a selected bandwidth above the cutoff frequency of the TE_{10} mode. The group velocity was determined from the computed incident field spectra and compared to the analytical expression [15, p. 425]; the agreement was excellent and demonstrated the quality of the numerical modal excitation.

The advantage of this approach to construct the excitation is that only the very low-level reflections from the absorbing boundary are retroreflected by the independent source in the auxiliary waveguide [5, pp. 110, 139], while the main algorithm is supplied with a robust, matched, and broad-band numerical excitation.

III. Experimental Validation of the Code

We demonstrate the ability of the subcell thin-wire formulation to account for the effective microwave properties of metal wires by comparing the measured and computed scattering parameters—in a standard S-band rectangular waveguide—for unit cells of wire hooks in their first resonance regime. The reflection (S_{11}) and transmission (S_{21}) coefficients can be determined accurately in a rectangular waveguide, and from them, through the law of energy conservation, the absorption spectra

$$P_{\mathrm{abs}} = \left[1 - \left(|S_{11}|^2 + |S_{21}|^2\right)\right] \times 100\%$$

with only the TE_{10} mode propagating. The unit cells were made of copper hooks and steel hooks, supported in slabs of polystyrene foam (to simulate "air"). In this paper, we only present results for the cranks shown in Fig. 1(a). More results for these and other unit cells, such as cells comprising staples, are presented in [2] and in detail in [1].

The unit cell was centred in an S-band rectangular waveguide, with the center legs in the direction of the waveguide axis (Fig. 3). A nominal half-wavelength resonance frequency of 2.8 GHz was selected for an isolated crank; this determined the total length of each wire as 54 mm, with each segment 18-mm long. The center legs were separated by 26 mm. The cranks were positioned in a polystyrene foam slab of dimensions 72 mm × 34 mm × 18 mm. The wire diameter was 300 μm for both the copper and steel (acoustic guitar string) cranks.

S-parameter measurements were performed with a Hewlett-Packard 8510C vector network analyzer measurement system. A schematic diagram of the measurement setup is shown in Fig. 5 [1]. Conservative estimates of the S_{11} and S_{21} measurement uncertainties are ≈0.1 dB in amplitude and ≈4° in-phase in the frequency range from approximately 2.3 to 3.95 GHz. In this band, only the TE_{10} mode can propagate in the waveguide.

In the numerical simulations, the frequency spectrum of the incident TE_{10} mode was 2.3–3.6 GHz. The performance of the PML (eight layers with a quadratic loss profile and theoretical reflection coefficient $R(0) = 10^{-7}$) was better than −75 dB in this frequency range. The reflected and transmitted E_y-fields were numerically sampled in the center of a transverse plane of the waveguide, approximately 200 mm from the front and back of the sample. The next higher order mode is

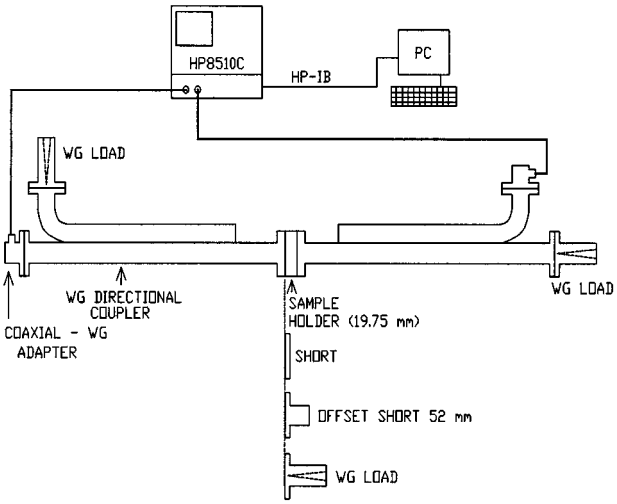

Fig. 5. Schematic diagram of the S-band rectangular waveguide measurement setup. The directional coupler to the right-hand side (port 2) was terminated in a high-quality waveguide load at the direct port and the transmitted signal was measured at the −10-dB directional port in order to suppress reflections from port 2 during measurement of S_{11}. An S_{11} one-port calibration was performed with three calibration standards and a through-calibration for the S_{21} measurement, with the sample holder in position [1].

evanescent and sufficiently attenuated at the sampling distance by a factor of 0.00016 at 3.6 GHz. The incident E_y-field was sampled in a simulation run for an empty waveguide, at the required positions to refer the phases of the calculated reflection and transmission coefficients to the sample front. The numerical simulations were executed at a discretization of $\Delta s = 1$ mm ($\Delta s \approx \lambda/76$ at the upper frequency limit of the TE_{10} mode) and $\Delta t = 1.926$ ps for 15 000 time steps. Typically, the waveguide size was $72 \times 34 \times 500$ cells.

The measured and computed scattering parameters are compared in Fig. 6 for the unit cells of copper and steel cranks in the essentially lossless host. The most prominent difference between the copper and steel unit cells is the increased absorption by the steel wires. The power dissipated by the copper unit cell was approximately 15% at resonance, both measured and predicted, as shown in Fig. 7. In sharp contrast, the steel unit cell dissipated approximately 70% of the power at resonance. The loss would not be predicted with the standard FDTD subcell thin-wire formulation in which the tangential E-field component on metallic conductors is assumed to be zero.

The dc conductivity of pure copper (5.7×10^7 S/m) was used in the numerical simulations of the copper unit cell ($r_0/\delta \approx 108$ at 2.3 GHz). The agreement between the measured and predicted scattering parameters for the copper unit cell is good, e.g., the discrepancy is less than 1% for the maximum reflection coefficient at resonance (Fig. 6).

The measured dc conductivity of the steel wire is 4.7×10^6 S/m. The relative permeability μ_r of magnetic steel is complex and dispersive at microwave frequencies [27]. We used an average $|\mu_r|$ across the S-band and included its effect as an effective conductivity $\sigma_{\mathrm{eff}} \approx \sigma_{\mathrm{wire}}/|\mu_r|$ in the internal impedance model $(Z_i)_{\mathrm{hf}} \approx (2\pi r_0)^{-1}\sqrt{j\omega\mu_0/\sigma_{\mathrm{eff}}}$. Various attempts to measure the effective properties of the steel string in the S-band were unacceptably inaccurate. (The measurement of the microwave properties of magnetic wires is an important practical

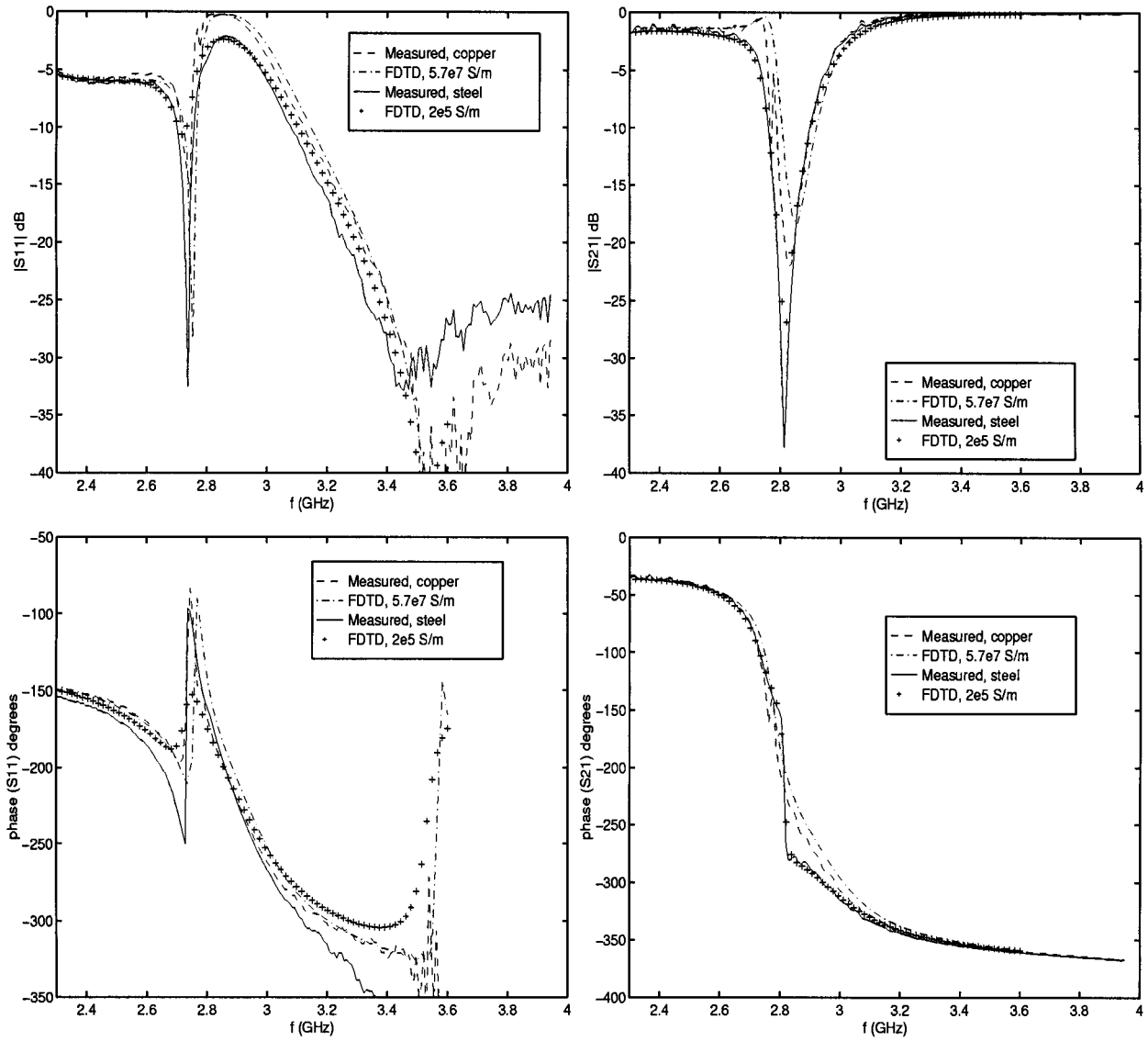

Fig. 6. Measured and predicted scattering parameters for copper ($\sigma_{\rm wire} = 5.7 \times 10^7$ S/m) and steel ($\sigma_{\rm eff} = 2 \times 10^5$ S/m) unit cells of cranks (chiral hooks) in polystyrene foam. The unit cells were illuminated in S-band rectangular waveguide. Calibration was with respect to the front of the sample.

problem, but will not be discussed here.) Instead, numerical simulation was used to establish that $\sigma_{\rm eff} = 2 \times 10^5$ S/m ($r_0/\delta \approx 150$ at 2.3 GHz) gives a good fit between the measured and predicted scattering parameters for the variety of steel unit cells we measured. This implies on average $|\mu_r| \approx 23.5$ across the frequency band, which is realistic for magnetic steel according to measurements by Sanderson [27, p. 42]. With this value, the measured and predicted maximum reflection coefficients at resonance were within 5% from each other (Fig. 6).

Away from resonance, both measurement and FDTD prediction did not distinguish significantly between the copper and steel unit cells—the differences were less than 2%.

The results from these and more experiments presented in [1] demonstrated that the subcell formulation—based on the local quasi-static $1/r$-field approximations and the high-frequency impedance model—provides a good model to predict the scattering and absorption by resonant three-segment hooks illuminated with the $\rm TE_{10}$ waveguide mode with the FDTD method.

IV. Experiments in Microwave Absorber

The experiments were also performed with the unit cells embedded in microwave absorber slabs [1], [2]. Fig. 8 shows the results for the unit cell in Fig. 1(a) embedded in the microwave absorber discussed earlier. The discrepancies between predicted and measured absorption spectra were of the order of 1%–5% with respect to maximum absorption, frequency of maximum absorption, bandwidth, and absorption away from resonance. Such differences were acceptable in the light of absorber inhomogeneities, manufacturing tolerance, and approximations in the numerical formulation. Neither measurement, nor computation showed marked differences between copper and steel when the wires were embedded in the absorbing host.

Some discussion on the motivation for the simulated structures is appropriate, although it is not the subject of this paper. Microwave absorbing materials find major practical application in radar cross-sectional reduction of aerospace and other

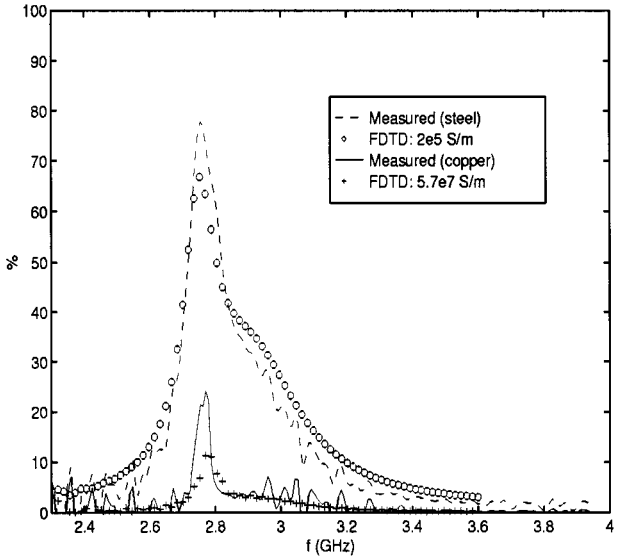

Fig. 7. Percentage power absorbed by copper and steel unit cells of cranks (chiral hooks) in polystyrene foam, an essentially lossless host. Measured data and FDTD predictions in an S-band rectangular waveguide.

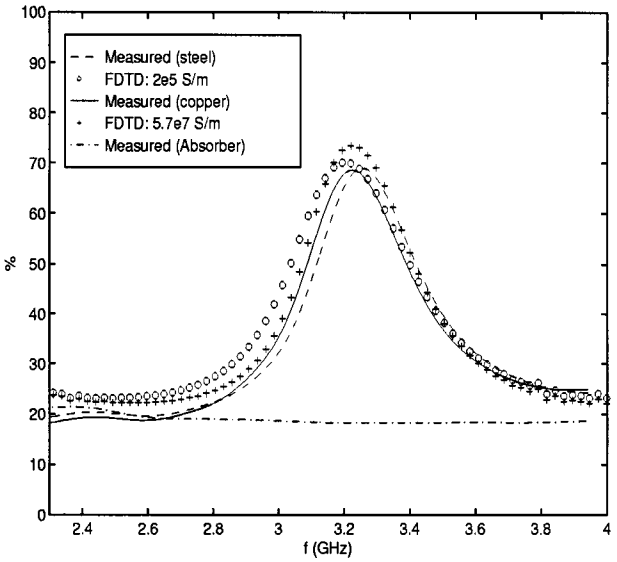

Fig. 8. As for Fig. 7, but with an absorbing dielectric as the host.

vehicles, electromagnetic interference (EMI) suppression, and antenna measurements. Much of the recent attention of microwave and antenna engineers to chiral materials was attracted by promises of a new superior class of microwave absorbers. We have investigated these claims by comparing the absorption of electromagnetic waves (in the S-band) by unit cells that are embedded in an absorbing dielectric host. The unit cells were designed to successively create chiral, racemic, and nonchiral materials [two of which are shown in Fig. 1(a) and (b)]. No physical mechanism was found to support patents that were filed from 1988 to 1992 or related claims in the engineering literature that chirality is the key to improved microwave absorbers. Instead, in synthetic composites that employ thin metal wires in a lossy dielectric host, half-wave resonance of the inclusions—not their geometric shape—was identified as the mechanism responsible for enhanced absorption [1], [2].

V. Conclusion

We account for the large—but finite—conductivity of physical metals by incorporating the high-frequency internal-impedance model for round conductors into the FDTD subcell thin-wire formulation of Umashankar *et al.* An effective conductivity is defined to model the increase in ohmic losses due to the high-frequency permeability of magnetic metals such as steel.

Our formulation has been verified against physical experiments of an S-band rectangular waveguide for both copper and steel wires. Good agreement was obtained between the measured and predicted scattering parameters for both magnitude and phase and the associated absorption spectra. The experiments with half-wave resonant copper and steel wires demonstrate that the effective finite conductivity of thin wires can introduce significant absorption about resonance. This is especially true in an otherwise transparent environment.

References

[1] M. Bingle, "The role of chirality in synthetic microwave absorbers," Ph.D. dissertation, Dept. Elect. Electron. Eng., Univ. Stellenbosch, Stellenbosch, South Africa, 1998.

[2] J. H. Cloete, M. Bingle, and D. B. Davidson, "The role of chirality and resonance in synthetic microwave absorbers," *Arch. Elektr. Uebertragung*, vol. 55, pp. 233–239, July/Aug. 2001.

[3] M. Bingle, D. B. Davidson, and J. H. Cloete, "FDTD simulation of scattering by conducting wires in rectangular waveguide," in *Proc. Antennas Propagat. Millennium Conf.*, vol. SP-444, Session 2A1–FDTD Applicat., Apr. 2000, CD-ROM.

[4] K. R. Umashankar, A. Taflove, and B. Beker, "Calculation and experimental validation of induced currents on coupled wires in an arbitrary shaped cavity," *IEEE Trans. Antennas Propagat.*, vol. AP-35, pp. 1248–1257, Nov. 1987.

[5] A. Taflove, *Computational Electrodynamics: The Finite-Difference Time-Domain Method*. Norwood, MA: Artech House, 1995.

[6] J. H. Cloete, S. A. Kuehl, and M. Bingle, "The absorption of electromagnetic waves at microwave frequencies by synthetic chiral and racemic materials," *Int. J. Appl. Electromagn. Mechan.*, vol. 9, pp. 103–114, 1998.

[7] J. Baker-Jarvis, R. G. Geyer, and P. D. Domich, "A nonlinear least-squares solution with causality constraints applied to transmission line permittivity and permeability determination," *IEEE Trans. Instrum. Meas.*, vol. 41, pp. 646–652, Oct. 1992.

[8] R. E. Diaz, "Application of the analytic theory of materials to the modeling of composites in electromagnetic engineering," in *Proc. 13th Annu. Rev. Progress Appl. Comput. Electromagn.*, Monterey, CA, Mar. 1997, pp. 766–773.

[9] A. G. Smith, "An experimental study of artificial isotropic chiral media at microwave frequencies," Dept. Elect. Electron. Eng., Ph.D. dissertation, Univ. Stellenbosch, Stellenbosch, South Africa, 1994.

[10] J. H. Cloete and A. G. Smith, "The constitutive parameters of a lossy chiral slab by inversion of plane wave scattering coefficients," *Microwave Opt. Technol. Lett.*, vol. 5, no. 7, pp. 303–306, 1992.

[11] ——, "Corrections to 'The constitutive parameters of a lossy chiral slab by inversion of plane wave scattering coefficients'," *Microwave Opt. Technol. Lett.*, vol. 7, no. 1, p. 42, 1994.

[12] A. Taflove, K. R. Umashankar, B. Beker, F. Harfoush, and K. S. Yee, "Detailed FD-TD analysis of electromagnetic fields penetrating narrow slots and lapped joints in thick conducting screens," *IEEE Trans. Antennas Propagat.*, vol. 36, pp. 247–257, Feb. 1988.

[13] J. J. Boonzaaier and C. W. I. Pistorius, "Finite-difference time-domain field approximations for thin wires with a lossy coating," *Proc. Inst. Elect. Eng.*, pt. H, vol. 141, no. 2, pp. 107–113, 1994.

[14] M. Douglas, M. Okoniewski, and M. A. Stuchly, "Accurate modeling of thin wire antennas in the FDTD method," *Microwave Opt. Technol. Lett.*, vol. 21, no. 4, pp. 261–265, 1999.

[15] S. Ramo, J. R. Whinnery, and T. van Duzer, *Fields and Waves in Communication Electronics*, 3rd ed. New York: Wiley, 1994.

[16] J. H. Beggs, R. J. Luebbers, K. S. Yee, and K. S. Kunz, "Finite-difference time-domain implementation of surface impedance boundary conditions," *IEEE Trans. Antennas Propagat.*, vol. 40, pp. 49–56, Jan. 1992.
[17] ——, "Corrections to 'Finite-difference time-domain implementation of surface impedance boundary conditions'," *IEEE Trans. Antennas Propagat.*, vol. 41, p. 118, Jan. 1993.
[18] E. Kreyszig, *Advanced Engineering Mathematics*, 6th ed. New York: Wiley, 1988.
[19] K. S. Kunz and R. J. Luebbers, *The Finite Difference Time Domain Method for Electromagnetics*. Boca Raton, FL: CRC Press, 1993.
[20] J.-P. Berenger, "A perfectly matched layer for the absorption of electromagnetics waves," *J. Comput. Phys.*, vol. 114, no. 1, pp. 185–200, 1994.
[21] D. S. Katz, E. T. Thiele, and A. Taflove, "Validation and extension to three dimensions of the Berenger PML absorbing boundary condition for FD-TD meshes," *IEEE Microwave Guided Wave Lett.*, vol. 4, pp. 268–270, Aug. 1994.
[22] E. A. Navarro, N. T. Sangary, and J. Litva, "Some considerations on the accuracy of the nonuniform FDTD method and its applications to waveguide analysis when combined with the perfectly matched layer technique," *IEEE Trans. Microwave Theory Tech.*, vol. 44, pp. 1115–1124, July 1996.
[23] Z. Wu and J. Fang, "Numerical implementation and performance of perfectly matched layer boundary condition for waveguide structures," *IEEE Trans. Microwave Theory Tech.*, vol. 43, pp. 2676–2683, Dec. 1995.
[24] J. P. Bérenger, "An effective PML for the absorption of evanescent waves in waveguides," *IEEE Microwave Guided Wave Lett.*, vol. 8, pp. 188–190, May 1998.
[25] F. Moglie, T. Rozzi, P. Marcozzi, and A. Schiavoni, "A new termination condition for the application of FDTD techniques to discontinuity problems in close homogeneous waveguide," *IEEE Microwave Guided Wave Lett.*, vol. 2, pp. 475–477, Dec. 1992.
[26] P. Alinikula and K. S. Kunz, "Analysis of waveguide aperture coupling using the finite-difference time-domain method," *IEEE Microwave Guided Wave Lett.*, vol. 1, pp. 189–191, Aug. 1991.
[27] A. E. Sanderson, "Effect of surface roughness on propagation of the TEM mode," in *Advances in Microwaves*, L. Young, Ed. New York: Academic, 1971, vol. 7, pp. 1–57.

Marianne Bingle was born in Pretoria, South Africa, in 1971. She received the B.Eng. degree (*cum laude*) in electrical and electronic engineering, M.Eng. degree (*cum laude*) in electronic engineering, and the Ph.D. degree from the University of Stellenbosch, Stellenbosch, South Africa, in 1993, 1995, and 1998, respectively.

She was a Post-Doctoral Researcher involved with the design of optical fibers at the Faculty of Electrical Engineering, Eindhoven University of Technology, Eindhoven, The Netherlands. In May 2002, she joined Electromagnetic Software and Systems (EMSS), Stellenbosch, South Africa. Her research interests include the measurement and computational modeling of electromagnetic properties of materials.

Dr. Bingle was the recipient of the URSI Young Scientist Awards presented at the 1998 International Symposium on Electromagnetic Theory, Thessaloniki, Greece, and at the 1999 General Assembly, Toronto, ON, Canada.

David Bruce Davidson (M'86) was born in London, U.K., 1961. He received the B.Eng. (*cum laude*), B.Eng. (*cum laude* and with honors), and M.Eng. degrees (*cum laude*) from the University of Pretoria, Pretoria, South Africa, in 1982, 1983, and 1986, respectively, and the Ph.D. degree from the University Stellenbosch, Stellenbosch, South Africa, in 1991.

Following national service (1984–1985) with the then South African Defence Force, he was with the Council for Scientific and Industrial Research, Pretoria, South Africa, prior to joining the University of Stellenbosch in 1988. He is currently a Professor at the University of Stellenbosch. He spent sabbaticals with the University of Arizona (1993) and Cambridge University (1997), where he was a Visiting Fellow with Trinity College. His main research interest is computational electromagnetics (CEM) and has authored or co-authored publications extensively on this topic. He was a Guest Editor for the *ACES Journal* "Special Issue on High-Performance Computing and CEM."

Dr. Davidson is a member of the Applied Computational Electromagnetic Society (ACES) and South African Institute of Electrical Engineers (SAIEE). He was a chairman of the IEEE Antennas and Propagation (AP)/Microwave Theory and Techniques (MTT) chapter of South Africa. He is joint editor of the *EM Programmer's Notebook* column of the *IEEE Antennas and Propagation Magazine*. He was a recipient of the South African FRD President's Award.

Johannes Hendrik Cloete (M'77) was born in Clocolan, South Africa, in 1945. He attended St. Andrew's School, Bloemfontein, South Africa. He received the B.Sc., B.Eng., and Ph.D. degrees from the University of Stellenbosch, Stellenbosch, South Africa, in 1969 and 1982, respectively, and the M.S.E.E. degree from the University of California at Berkeley, in 1972.

From 1969 to 1983, he was with the South African Navy, the National Institute for Defence Research, Pretoria, South Africa, Scientific-Atlanta Inc., Atlanta, GA, and the University of Pretoria, South Africa. Since 1984, he has been a Professor of electrical and electronic engineering at the University of Stellenbosch. His research interests include electromagnetic wave phenomena (radiation, propagation, absorption, scattering, guiding) in stratified, dispersive matter, properties of matter at radio and microwave frequencies, and antenna design. He collaborates with Sydney University to introduce long-range borehole-radar technology into the South African mining industry for delineation and imaging of ore bodies and fault structures in *inter alia* the Witwatersrand basin (gold), the Bushveld igneous complex (platinum group metals), and diamantiferous systems.